QUEEN'S UNIVERSITY BELFAST

# Hemispheric black carbon increase after the 13th-century Māori arrival in New Zealand

McConnell, J., Chellman, N. J., Mulvaney, R., Eckhardt, S., Stohl, A., Plunkett, G., Kipfstuhl, S., Freitag, J., Isaksson, E., Gleason, K. E., Brugger, S. O., McWethy, D. B., Abram, N. J., Liu, P., & Aristarain, A. J. (2021). Hemispheric black carbon increase after the 13th-century Māori arrival in New Zealand. *Nature*, *598*, 82–85. https://doi.org/10.1038/s41586-021-03858-9

**Published in:**
Nature

**Document Version:**
Peer reviewed version

**Queen's University Belfast - Research Portal:**
Link to publication record in Queen's University Belfast Research Portal

**Publisher rights**
Copyright 2021, the Authors.
This work is made available online in accordance with the publisher's policies. Please refer to any applicable terms of use of the publisher

**General rights**
Copyright for the publications made accessible via the Queen's University Belfast Research Portal is retained by the author(s) and / or other copyright owners and it is a condition of accessing these publications that users recognise and abide by the legal requirements associated with these rights.

**Take down policy**
The Research Portal is Queen's institutional repository that provides access to Queen's research output. Every effort has been made to ensure that content in the Research Portal does not infringe any person's rights, or applicable UK laws. If you discover content in the Research Portal that you believe breaches copyright or violates any law, please contact openaccess@qub.ac.uk.

**Open Access**
This research has been made openly available by Queen's academics and its Open Research team. We would love to hear how access to this research benefits you. – Share your feedback with us: http://go.qub.ac.uk/oa-feedback

Download date:19. Apr. 2024

# Hemispheric black carbon increase after 13th C Māori arrival in New Zealand

Joseph R. McConnell[1,*], Nathan J. Chellman[1], Robert Mulvaney[2], Sabine Eckhardt[3], Andreas Stohl[4], Gill Plunkett[5], Sepp Kipfstuhl[6], Johannes Freitag[6], Elisabeth Isaksson[7], Kelly E. Gleason[8], Sandra O. Brugger[1], David B. McWethy[9], Nerilie J. Abram[10,11,12], Pengfei Liu[13,14], and Alberto J. Aristarain[15]

[1]Division of Hydrologic Sciences, Desert Research Institute, Reno, NV 89512, USA

[2]British Antarctic Survey, Natural Environment Research Council, Cambridge CB3 0ET, United Kingdom

[3]Department of Atmospheric and Climate Research, Norwegian Institute for Air Research, N-2027, Norway

[4]Department of Meteorology and Geophysics, University of Vienna, 1090 Vienna, Austria

[5]School of Natural and Built Environment, Queen's University Belfast, BT7 1NN Belfast, United Kingdom

[6]Alfred-Wegener-Institut Helmholtz-Zentrum für Polar- und Meeresforschung, 27570 Bremerhaven, Germany

[7]Norwegian Polar Institute, Fram Centre, N-9296 Tromsø, Norway

[8]Department of Environmental Science and Management, Portland State University, Portland, OR 97207, USA

[9]Department of Earth Sciences, Montana State University, Bozeman, MT 59717, USA

[10]Research School of Earth Sciences, Australian National University, Canberra, ACT 2602, Australia

[11]ARC Centre of Excellence for Climate Extremes, Australian National University, Canberra ACT 2602, Australia.

[12]Australian Centre for Excellence in Antarctic Science, Australian National University, Canberra ACT 2602, Australia.

[13]School of Earth and Atmospheric Sciences, Georgia Institute of Technology, Atlanta, GA 30332, USA

[14]School of Engineering and Applied Sciences, Harvard University, Cambridge, MA 02138, USA

[15]Instituto Antártico Argentino, Centro Regional de Investigaciones Cientifícas y Teconológicas, 5500 Mendoza, Argentina (retired)

[*]**Corresponding Author**

Joseph R. McConnell, Desert Research Institute, 2215 Raggio Parkway, Reno NV 89512 USA (Email: Joe.McConnell@dri.edu; Phone: 775-673-7348; Fax: 775-673-7363)

**New Zealand was among the last habitable places on earth to be colonized by humans [1]. Charcoal records indicate that wildfires were rare prior to human arrival and widespread following 13th to 14th C Māori settlement [2], but the precise timing and magnitude of associated biomass-burning emissions are unknown [1,3], as are effects on light-absorbing black carbon and other aerosol concentrations over the pristine South Pacific, Southern Ocean, and Antarctica [4]. Here we used a broad array of accurately dated Antarctic ice-core records to show that while black carbon concentrations and deposition rates were approximately stable over continental Antarctica during the Common Era, they were 2- to 3-fold higher over the northern Antarctic Peninsula during the past 700 years. Aerosol modeling [5] demonstrates that the observed deposition pattern could have resulted only from increased emissions poleward of 40°S – implicating fires in Tasmania, New Zealand, and Patagonia – but only New Zealand paleofire records indicate a coincident increase in biomass burning. Rapid increases in deposition started in 1297 (±30) in the northern Antarctic Peninsula, consistent with late-13th C Māori settlement and New Zealand black carbon emissions of 36 (±21) Gg/y during peak deposition in the 16th C. While charcoal and pollen records suggest earlier, climate-modulated burning in Tasmania and southern Patagonia [6,7], the deposition pattern from the Antarctic ice-core array shows that black carbon emissions from Māori burning dwarfed other preindustrial emissions during the past 2000 years, providing clear evidence of large-scale environmental effects from early human activities across the remote Southern Hemisphere.**

Incomplete understanding of preindustrial atmospheric aerosol sources and concentrations, including biomass burning (BB) aerosols [8,9], limits large-scale climate model projections because even small changes may have profound effects on radiative forcing [10,11]. The primary light-absorbing constituent is refractory black carbon (rBC) resulting from incomplete combustion during BB and, more recently, fossil fuel burning. Combustion also emits organic carbon and other aerosols that act as cloud condensation nuclei and alter cloud properties [9], while providing bioavailable micro-nutrients such as iron to remote ocean regions [12].

The modern atmosphere over the higher southern latitudes is among the most pristine on Earth [4] so quantifying past changes in atmospheric rBC and other BB aerosols in the region potentially is important to understanding large-scale radiative forcing [11] and carbon sequestration linked to fertilization of the micro-nutrient-limited Southern Ocean [12,13]. Reconstructing past BB frequently is based on proxy paleofire records such as charcoal deposition in lake sediments [2,14] and records from the higher southern latitudes generally suggest order-of-magnitude variations in natural, climate-modulated BB especially during the first millennium [6,7], while New Zealand records suggest large changes in prehistoric anthropogenic BB [2]. Quantifying atmospheric aerosol emissions from such local records is highly uncertain, however, and more direct proxies of past aerosol concentrations come from measurements of BB indicators in glacier ice [15,16]. Here we used a broad Antarctic array of well-dated records from ice cores and aerosol transport modeling to investigate atmospheric rBC concentrations over the northern Antarctic Peninsula (nAP) and much of continental Antarctica during the Common Era. The atmospheric lifetime of rBC aerosols typically is on the order of a few days and proxy records are sensitive to emissions from specific areas. These cores were collected thousands of kilometers from potential sources so the records reflect large-scale BB emissions and provide robust proxies of atmospheric concentrations and deposition changes over vast regions of the South Pacific, Southern Ocean, and Antarctica.

High-resolution chemical and elemental measurements of concentration and depositional flux (Extended Data Fig. 1, Methods) were made in six Antarctic ice cores (Extended data Table 1) using the unique continuous ice-core analytical system at the Desert Research Institute (DRI) [9,15,17]. The array extends from 64$^{o}$S to 82$^{o}$S (Fig. 1) and consists of two cores from James Ross Island (JRI) representing the nAP and four cores from continental Antarctica representing lower-latitude Dronning Maud Land (DML) and higher-latitude interior East Antarctic Plateau (iEAP) regions. Age scales are consistent with the WD2014 chronology [18] (Methods), with estimated uncertainties (1σ) less than ±5 years during the Common Era but somewhat higher (±20 years) during the 1$^{st}$ millennium in the nAP record dated with ice flow modeling (Methods). Measurements show that rBC deposition varied substantially over Antarctica during the past 2000 years, with a marked divergence between the nAP and continental Antarctica starting in the late 13$^{th}$ C that has persisted to present (Fig. 1). Although different in magnitude between the northern and southern sites, rBC deposition at all the ice-

core sites generally was low, relatively stable, and approximately covarying prior to the 1200s. For example, fluxes averaged 59.3 (±0.9 SE), 19.8 (±0.4 SE), and 5.8 (±0.1 SE) $\mu g/m^2/y$ between 900 and 1200 in the nAP, DML, and iEAP records, respectively. The nAP and continental records sharply diverged after the late 13$^{th}$ C, with deposition in the nAP increasing between 1500 and 1600 to >250% of the 900 to 1200 average, and decreasing 10 to 35% in the DML and iEAP records. Deposition in the nAP declined between 1600 and 1650, increased again between 1650 and 1700 ,and then declined but remained well above the levels at the start of the millennium. Except for small increases during the 19$^{th}$ C, low rBC deposition in continental Antarctica generally persisted after 1600.

Scavenging and deposition during long-range atmospheric transport of rBC aerosols from potential source regions to Antarctica resulted in the observed order-of-magnitude differences in overall rBC deposition rates at the nAP, DML, and iEAP sites and provide insight into possible BB source regions and their changes. Simulations with the FLEXPART [5,19] atmospheric aerosol transport and deposition model were used to investigate these sources (Methods). Prior to the late 13$^{th}$ C divergence in rBC deposition, the average nAP/DML and nAP/iEAP deposition ratios in the ice (900 to 1200) were 3.0 (±0.1 SE) and 10.1 (±0.2 SE), respectively, and surprisingly consistent during the first 1300 years (Fig. 1). To identify possible source regions consistent with the 3.0 average nAP/DML ratio observed in the ice, we isolated areas of the Southern Hemisphere (SH) where the nAP/DML ratio in FLEXPART emission sensitivities is between 2 and 5 (Fig. 2) to allow for ~60% uncertainty in the simulations (Methods). This bracketed area encompasses most of the SH land area between 15 and 40$^{o}$S, including many of the modern BB regions in South America and Africa, so the observed spatial pattern of rBC deposition in Antarctica prior to the late 13$^{th}$ C divergence is consistent with emissions from across much of the mid-latitude SH. The regions where the nAP/iEAP ratio is between 5 and 15 (Extended data Fig. 2) encompasses much of the same area. Emission sensitivity ratios between ice-core sites for potential BB areas poleward of 40$^{o}$S, however, are much too high and significant variations in rBC emissions before the 14$^{th}$ C would be inconsistent with the relatively constant nAP/DML and nAP/iEAP deposition ratios observed in the ice. Using the simplifying assumption that rBC emissions were approximately equivalent across the 15 to 40$^{o}$S region and average emission sensitivities of 11.3, 2.0, and 0.6 $(\mu g/m^2/y)/(kg/s)$ for the nAP, DML, and iEAP, respectively, we estimate average 900 to 1200 emissions of 186, 312, and 305 Gg/y. These are comparable to 1750 to 1799 average estimates of 218 Gg/y from open BB in the same 15 to 40$^{o}$S region [20] used here as a rough approximation of preindustrial BB emissions.

The ice records show that peak rBC deposition in the nAP occurred in the 16$^{th}$ and 17$^{th}$ C. Deposition in the nAP was 10.8 (±0.2 SE) times that in DML during the 16$^{th}$ C and 30.4 (±0.5 SE) times that in the iEAP (Fig. 1) – or more than 3 times the 3.0 (±0.1 SE) and 10.1 (±0.2 SE) ratios observed in the ice earlier – indicating one or more additional rBC sources from regions where the nAP/DML and nAP/iEAP emission sensitivity ratios are high (>>10 and >>30). In the

FLEXPART simulations, only BB regions poleward of 40°S (i.e., Tasmania, New Zealand, and southern Patagonia) have nAP/DML emission sensitivity ratios >10 (Fig. 2), and only New Zealand and Patagonia have nAP/iEAP ratios >30 (Extended data Fig. 2).

Paleofire records from Patagonia and Tasmania (Fig. 1), and modeling indicate that BB prior to European colonization was driven primarily by large-scale climate variations [21,22], and that BB in both regions was low for much of the past 700 years when the climate in Patagonia and Tasmania was relatively wet [6,7] (Fig. 1). Indigenous hunter-gatherer populations had been living in Tasmania and Patagonia for millennia prior to European arrival and probably used small-scale fires for land management [7,23,24]. However, there is little historical or proxy evidence of large changes in anthropogenic BB prior to European settlement in the 19$^{th}$C.

New Zealand was among the last habitable places on Earth to be colonized by humans and charcoal-based fire records indicate a very different BB history than Tasmania and Patagonia. Wildfire was absent or insignificant prior to about 1300 but widespread during the past 700 years (Fig. 1), with pronounced increases in fire occurrence attributed to arrival and colonization of New Zealand by the Māori and their use of fire for land clearing and management [2,25]. However, the precise chronology of BB onset in New Zealand is limited by uncertainties in the lake-sediment age scales as well as watershed-to-watershed variability, while the chronology and nature of Māori arrival in New Zealand is poorly constrained in archaeological and other records. Estimated arrival dates based on radiocarbon dating vary from the early-13$^{th}$ C to the 14$^{th}$ C [1,3], and the estimated foundational population arriving in New Zealand varies from a few tens of explorers to hundreds of settlers as part of a planned mass migration [3]. Evaluation of the well-dated Antarctic ice-core records using the break function regression algorithm BREAKFIT [26] indicates that widespread BB emissions from New Zealand began in 1297 (±30) (Fig. 1, Methods). Enhanced rBC deposition in the nAP increased approximately linearly, not exponentially, during the 14$^{th}$ C to 16$^{th}$ C and early increases were especially sharp (Fig. 1), seemingly consistent with mass migration and a large founding population rather than growth of a small resident population [3].

To estimate the magnitude of the emissions from Māori BB, we subtracted from the nAP record the DML and iEAP records scaled by 3.0 and 10.1, respectively (Fig. 1), with the scale factors determined by matching average 900 to 1200 rBC deposition. Differences between the nAP and two scaled continental records were nearly identical (Fig. 1), with average enhanced fluxes of 100.2 (±2.8 SE) and 110.9 (±2.6 SE) μg/m$^2$/y from 1500 to 1600 at the end of the initial Māori burning period for nAP-DML and nAP-EAP, respectively, so estimates of enhanced rBC deposition are within 3.5% of the average 104.6 (±2.7 SE) μg/m$^2$/y regardless of which continental record is used as background.

We also subtracted the similarly scaled FLEXPART emission sensitivities for DML and iEAP from the nAP sensitivities to estimate the New Zealand emissions required to generate the enhanced rBC deposition in the nAP (Fig. 2). Using the emission sensitivity for New Zealand of

91 (±55 to account for the assumed 60% uncertainty) ($\mu g/m^2/y$)/(kg/s), the average observed 104.6 $\mu g_{rBC}/m^2/y$ enhancement during the 16th C corresponds to 36 (±21) Gg/y (1.1 kg/s). Although highly variable between different inventories, recent (2003 to 2019) estimates of rBC emissions from New Zealand range from <1 Gg/y for the Global Fire Emissions Database (GFEDv4s) to 21 (±8) Gg/y for the Quick Fire Emissions Dataset (QFEDv2.5r1) [27] so the 36 (±21) Gg/y estimate during the 16th C is between ~2 and ~40 times recent emissions inventories. This seems plausible given that New Zealand forest cover today is only 25-30%, while forest cover was 85-90% when the Māori arrived. Lacking a natural fire cycle, fuel probably had accumulated for millennia [28]. Forward simulations with FLEXPART based on postulated New Zealand emissions of 36 $Gg_{rBC}/y$ show pronounced increases in atmospheric concentration and deposition in an annulus around the Antarctic continent (Fig. 3), with the highest increases over the South Pacific.

Aerosol-enabled Earth System models require detailed information on past climate for model evaluation [10], including emissions and atmospheric concentrations of light-absorbing rBC and other nutrient-rich BB aerosols [12,13]. The ice-core records of rBC deposition presented here directly reflect aerosol concentrations over large regions of the South Pacific, Southern Ocean, and Antarctica during the Common Era and document a persistent, 2- to 3-fold increase in the nAP starting in 1297 (±30). All evidence suggests that this pronounced, rapid increase was the result of large-scale Māori migration and the start of widespread anthropogenic BB in New Zealand more than 7000 km away that resulted in estimated emissions of 36 (±21) Gg/y during the 16th C maximum.

The evolution of natural and anthropogenic BB poleward of 40°S suggested by charcoal records is substantially different than the rBC concentration and deposition history recorded in the Antarctic ice cores, illustrating the challenges of inferring atmospheric BB emissions from local paleofire records. First, the New Zealand charcoal records suggest a rapid initial increase in BB that peaked in the 15th C, a decline to the early 17th C, and then a similar peak in the mid-19th C (Fig. 1). The rBC history documented in the ice records indicates the same initial rise in emissions but peak rBC deposition in the nAP in the 16th C and 17th C occurred when the charcoal records suggest lower BB in New Zealand. Second, rBC emissions from Tasmania and Patagonia located at the same latitude as New Zealand will be entrained in the westerly winds, resulting in increased atmospheric concentrations and deposition rates in a similar annular ring around Antarctica (Fig. 3). Although significant BB emissions might be inferred from Patagonian and Tasmanian lake-sediment records that show orders-of-magnitude changes in charcoal deposition prior to the 13th C [6,7] (Fig. 1), the ice-core history indicates no significant changes in rBC emissions poleward of 40°S during this period (Fig. 1). Using the FLEXPART emission sensitivities and the variability in the nAP/DML and nAP/iEAP deposition ratios in the ice before and after the late 13th C divergence, we estimate that BB emissions from southern Patagonia (>50°S) and Tasmania were no more than 2.8 Gg/y and 5.7 Gg/y, respectively (Methods) – or 8 to 16% of the 36 (±22) Gg/y estimated from Māori BB during the 16th C. This indicates that

anthropogenic rBC emissions from New Zealand dwarfed earlier climate-driven BB emissions in Tasmania and Patagonia and providing clear evidence of hemispheric-scale environmental impacts on the remote SH from early human activities.

## References


1 Wilmshurst, J. M., Hunt, T. L., Lipo, C. P. & Anderson, A. J. High-precision radiocarbon dating shows recent and rapid initial human colonization of East Polynesia. *Proceedings of the National Academy of Sciences* **108**, 1815, doi:10.1073/pnas.1015876108 (2011).

2 McWethy, D. B. *et al.* Rapid landscape transformation in South Island, New Zealand, following initial Polynesian settlement. *Proceedings of the National Academy of Sciences* **107**, 21343, doi:10.1073/pnas.1011801107 (2010).

3 Walter, R., Buckley, H., Jacomb, C. & Matisoo-Smith, E. Mass Migration and the Polynesian Settlement of New Zealand. *Journal of World Prehistory* **30**, 351-376, doi:10.1007/s10963-017-9110-y (2017).

4 Remer, L. A. *et al.* Global aerosol climatology from the MODIS satellite sensors. *Journal of Geophysical Research: Atmospheres* **113**, doi:10.1029/2007JD009661 (2008).

5 Stohl, A., Forster, C., Frank, A., Seibert, P. & Wotawa, G. Technical note: The Lagrangian particle dispersion model FLEXPART version 6.2. *Atmospheric Chemistry and Physics* **5**, 2461-2474 (2005).

6 Moreno, P. I. *et al.* Southern Annular Mode-like changes in southwestern Patagonia at centennial timescales over the last three millennia. *Nature Communications* **5**, 4375, doi:10.1038/ncomms5375 (2014).

7 Fletcher, M.-S. *et al.* Centennial-scale trends in the Southern Annular Mode revealed by hemisphere-wide fire and hydroclimatic trends over the past 2400 years. *Geology* **46**, 363-366, doi:10.1130/G39661.1 (2018).

8 Hamilton, D. S. *et al.* Reassessment of pre-industrial fire emissions strongly affects anthropogenic aerosol forcing. *Nature Communications* **9**, 3182, doi:10.1038/s41467-018-05592-9 (2018).

9 Liu, P. *et al.* Improved estimates of preindustrial biomass burning reduce the magnitude of aerosol climate forcing in the Southern Hemisphere. *Science Advances* **7**, eabc1379, doi:10.1126/sciadv.abc1379 (2021).

10 Carslaw, K. S. *et al.* Large contribution of natural aerosols to uncertainty in indirect forcing. *Nature* **503**, 67-71, doi:10.1038/nature12674 (2013).

11 Carslaw, K. S. *et al.* Aerosols in the Pre-industrial Atmosphere. *Current Climate Change Reports* **3**, 1-15, doi:10.1007/s40641-017-0061-2 (2017).

12 Matsui, H. *et al.* Anthropogenic combustion iron as a complex climate forcer. *Nature Communications* **9**, 1593, doi:10.1038/s41467-018-03997-0 (2018).

13 Moore, C. M. *et al.* Processes and patterns of oceanic nutrient limitation. *Nature Geoscience* **6**, 701-710, doi:10.1038/ngeo1765 (2013).

14 Marlon, J. R. *et al.* Climate and human influences on global biomass burning over the past two millennia. *Nature Geoscience* **1**, 697-702, doi:10.1038/ngeo313 (2008).

15 McConnell, J. R. *et al.* 20th-century industrial black carbon emissions altered arctic climate forcing. *Science* **317**, 1381-1384, doi:10.1126/science.1144856 (2007).

16 Arienzo, M. M. *et al.* Holocene black carbon in Antarctica paralleled Southern Hemisphere climate. *Journal of Geophysical Research: Atmospheres* **122**, 6713-6728, doi:10.1002/2017JD026599 (2017).

17 McConnell, J. *et al.* Synchronous volcanic eruptions and abrupt climate change ~17.7 ka plausibly linked by stratospheric ozone depletion. *Proceedings of the National Academy of Sciences of the United States of America* **114**, 10035-10040, doi:10.1073/pnas.1705595114 (2017).

18 Sigl, M. *et al.* The WAIS Divide deep ice core WD2014 chronology - Part 2: Annual-layer counting (0-31 ka BP). *Clim. Past* **12**, 769-786, doi:10.5194/cp-12-769-2016 (2016).

19 Eckhardt, S. *et al.* Source-receptor matrix calculation for deposited mass with the Lagrangian particle dispersion model FLEXPART v10.2 in backward mode. *Geophys Model Dev* **10**, 4605-4618, doi:10.5194/gmd-10-4605-2017 (2017).

20 van Marle, M. J. E. *et al.* Historic global biomass burning emissions for CMIP6 (BB4CMIP) based on merging satellite observations with proxies and fire models (1750–2015). *Geosci. Model Dev.* **10**, 3329-3357, doi:10.5194/gmd-10-3329-2017 (2017).

21 Iglesias, V. & Whitlock, C. Fire responses to postglacial climate change and human impact in northern Patagonia (41–43°S). *Proceedings of the National Academy of Sciences* **111**, E5545, doi:10.1073/pnas.1410443111 (2014).

22 Neukom, R. *et al.* Multiproxy summer and winter surface air temperature field reconstructions for southern South America covering the past centuries. *Climate Dynamics* **37**, 35-51, doi:10.1007/s00382-010-0793-3 (2011).

23 Mundo, I. A. *et al.* Fire history in southern Patagonia: human and climate influences on fire activity in Nothofagus pumilio forests. *Ecosphere* **8**, e01932, doi:10.1002/ecs2.1932 (2017).

24 Stahle, L. N., Whitlock, C. & Haberle, S. G. A 17,000-Year-Long Record of Vegetation and Fire from Cradle Mountain National Park, Tasmania. *Frontiers in Ecology and Evolution* **4**, 82 (2016).

25 McWethy, D. B., Whitlock, C., Wilmshurst, J. M., McGlone, M. S. & Li, X. Rapid deforestation of South Island, New Zealand, by early Polynesian fires. *The Holocene* **19**, 883-897, doi:10.1177/0959683609336563 (2009).

26 Mudelsee, M. Break function regression. *European Physical Journal-Special Topics* **174**, 49-63, doi:10.1140/epjst/e2009-01089-3 (2009).

27 Liu, T. *et al.* Diagnosing spatial biases and uncertainties in global fire emissions inventories: Indonesia as regional case study. *Remote Sensing of Environment* **237**, 111557, doi:10.1016/j.rse.2019.111557 (2020).

28 Perry, G. L. W., Wilmshurst, J. M. & McGlone, M. S. Ecology and long-term history of fire in New Zealand. *New Zealand Journal of Ecology* **38**, 157-176 (2014).

**Figure 1 | Proxy records of SH biomass burning during the Common Era showing ~3-fold higher BB aerosol deposition over the nAP starting in the 14$^{th}$ C and lower levels in continental Antarctica.** rBC deposition records from **a,** nAP and DML, and **b,** nAP and iEAP. **c,** Individual and average differences between the nAP and scaled DML and iEAP records, with the date of the divergence between nAP and continental records objectively determined to be 1297 (±30) using BREAKFIT [26]. **d,** Deposition ratios between nAP and DML and iEAP. **e,** Individual and average standardized lake-sediment charcoal records from New Zealand's South Island [2]. **f,** Tasmanian and southern Patagonian charcoal records illustrating linkages with large-scale climate variations [6,7]. Also shown are the ~1325 settlement of New Zealand by the Māori [3], the subsequent Initial Burning Period [2], and the ~1840 start of European colonization. Inset shows the locations of ice cores in the Antarctic rBC array.

**Figure 2 | Simulated emission sensitivities. a,** nAP. **b,** DML. **c,** nAP/DML. **d,** nAP-DML$_{scaled}$, where the DML scaler of 3.0 is the average nAP/DML ratio in the ice cores from 900 to 1200. Insets show values for New Zealand and crosses mark ice-core locations.

**Figure 3 | Simulated, 16$^{th}$ C rBC deposition from postulated average emissions of 36 Gg/y from anthropogenic burning in New Zealand that tripled rBC aerosol flux over the nAP.** Crosses mark ice-core locations.

## Methods

**Antarctic Ice-Core Array:** The cores (Extended data Table 1) used in this study were: (1) the 363.9-m JRI_2008 core collected in 2008 by the British Antarctic Survey from James Ross Island located at the northern tip of the Antarctic Peninsula [29,30], (2) a 38-m section of the 121.9-m JRI_D98 core collected in 1998 from James Ross Island by the Instituto Antártico Argentino [31], 3) the 200-m B40 [16,32] and B53 [9] cores collected from continental East Antarctica in 2013 by the Alfred Wegener Institute , and 4) the 90.6-m NUS07_7 and 80.3-m NUS08_7 cores [32,33] collected from continental East Antarctica in 2008 and 2009, respectively, as part of the Norwegian-United States IPY Scientific Traverse of East Antarctica.

**rBC and other aerosol measurements:** High-depth-resolution measurements of a broad range of more than 30 elements, chemical species, and isotopes were made in all six cores using the continuous ice-core analytical system at the Desert Research Institute (DRI) and well-established methods [9,17,34]. rBC mass concentrations (Extended Data Fig. 1) were measured using the Single Particle Soot Photometer (SP2)-based method developed at DRI [15]. Sulfur and sodium mass concentrations that underpinned annual layer counting and volcanic synchronization were measured using Inductively Coupled Plasma-Mass Spectrometry [17,34]. Ammonium concentration also used for annual layer counting in the JRI cores was measured using fluorescence spectrometry. Estimated uncertainties in concentration measurements were <10%. Recent rBC concentrations in the JRI_2008 core were confirmed using SP2-based measurements made nearly a decade earlier in a 38-m section of the JRI_D98 core collected nearby (Extended data Fig. 1).

To verify rBC and other measurements made months or years apart, 1-m replicate sections from previously analyzed cores typically are measured in the DRI ice-core lab at the start of each day during an analytical campaign. For the JRI_2008 analysis campaign that occurred over 13 days in January and February, 2016, replicate sections from the B40 core were measured each day and compared to the original B40 measurements made in autumn, 2013. Comparisons show excellent agreement (Extended data Fig. 3) and confirm differences in rBC concentrations and deposition rates between the nAP and DML, as well as the marked changes in rBC in the JRI_2008 core during the 2$^{nd}$ millennium.

**Ice-core chronologies:** We used multi-parameter annual layer counting [18,35], constrained by volcanic tie points to the well-dated WAIS Divide sulfur record on the WD2014 age scale, to develop chronologies for the cores collected from higher snow accumulation sites (i.e., JRI_2008, JRI_D98, B40, and NUS08_7). Absolute uncertainty in WD2014 during the Common Era generally is <3 years since it is based on annual layer counting constrained by numerous volcanic and cosmogenic nuclide tie points to tree ring chronologies that are assumed to be absolutely dated [36]. Moreover, new unpublished cosmogenic nuclide measurements in B53 and WAIS Divide ice indicate an error of <2 years in the WD2014 chronology at the recently discovered cosmogenic nuclide event that occurred 2610 years before 1950 (yBP) [37].

Seasonally varying parameters used for annual layer counting were different between cores but generally included sulfur to sodium ratios, stable water isotope ratios, and ammonium concentrations. For cores collected from low snowfall sites (i.e., B53, NUS07_7), dating relied exclusively on volcanic synchronization to WAIS Divide, with volcanic tie points based on sulfur concentration peaks approximately every 25 years [33].

Previous high-resolution measurements in the JRI_2008 core necessary for annual layer counting extended only to ~130 m corresponding to ~1807, so dating of the record below that on the JRI1 chronology was based on ice flow modeling alone [30]. Using new continuous chemical and elemental measurements made with the DRI analytical system spanning the entire 363.9-m core, here we extended annual layer counting to ~300 m (Extended data Fig. 4), resulting in substantial revision of the JRI1 chronology below ~130 m.

Unlike the continental Antarctic cores, high background variability in marine biogenic sulfur limited the reliability of volcanic synchronization in the JRI_2008 record, while surface melt, percolation, and flow thinning restricted annual layer counting to the upper 82% of the JRI_2008 core corresponding to the period ~1000 to 2008 on the revised age scale. Therefore, the chronology for the deepest part of the JRI_2008 record was developed using ice flow modeling constrained by sulfur-based volcanic synchronization in the layer-counted section and tephra geochemistry-based volcanic synchronization and distinct water isotope variations deeper in the core. Because uncertainties in annual layer counting increased below ~1200, we used eight tie points from the annual layer counted section, with the deepest being the distinct sulfur fallout from the 1258 Samalas eruption. Age control points above this included the surface when drilling was conducted in 2008, the 1953 start of atmospheric thermonuclear testing in the SH clearly identified in continuous plutonium measurements [38], and fallout from five large volcanic eruptions (Extended data Figs. 5, 6).

To constrain the age scale in the deeper JRI_2008 record, we used distinct changes in water isotopes linked to the Antarctic Cold Reversal (Extended data Fig. 6), as well as new geochemical fingerprinting of tephra extracted from a visible layer located at 345.43 m (95% of total depth). Tephra shards were sent to Queen's University Belfast for geochemical analysis where the sample was prepared using protocols described previously [39]. Major element geochemistry was determined on a JEOL FEGSEM 6500F using combined electron and wavelength dispersive spectrometry, with secondary glass standards analyzed in the same sessions to ensure acceptable operating conditions. Eleven major and minor elements were analyzed, with all measurements normalized to 100% to allow for water content. The tephra geochemistry suggests a source in the South Sandwich Islands. Comparisons to previously published tephra extracted from Antarctic ice (Extended data Fig. 7) identified a match to the Vostok tephra reported previously at 132.6 m in the EDC96 core from Dome Concordia (75.1$^{o}$S, 123.4$^{o}$E) [40] and in a number of Vostok (78.5$^{o}$S, 106.8$^{o}$E) cores including at 103.14 m in the vk_BH1 core [41]. We determined a tephra deposition date of 3568 yBP on the WD2014 age scale by synchronizing high-resolution sulfate measurements in EDC96 [42] to sulfate measurements in

WAIS Divide [43]. The final revised age scale (Extended data Fig. 6) was composed of the volcanically constrained annual layer counting results from the surface to the 1258 Samalas event and the constrained flow model results from 1258 to the bottom. Co-variability in the JRI_2008 and DML rBC deposition records from 1 to 1100 (Fig. 1) suggests that the new JRI_2008 age scale is reliable throughout the Common Era.

**Depositional rBC fluxes:** Following standard procedures, depositional fluxes in the continental Antarctic cores were calculated by multiplying the annually-averaged concentrations by water-equivalent accumulation rates corrected for flow thinning as necessary. For the DML cores dated with volcanically constrained annual layer counting, we used flow-corrected annual layer thicknesses. For the volcanically synchronized iEAP cores, we used the recent average water equivalent accumulation rates (Extended data Table S1). For both DML and iEAP cores, accumulation rates generally varied by less than ±10% during the Common Era. For the deep JRI_2008 core where the upper 2000 years of the record extend over more than 90% of the ice thickness, we used a smoothly varying fit to the annual accumulation rates derived from the ice flow model (Extended Data Fig. 6). The average water-equivalent accumulation was 699 kg/m$^2$/y and ranged from 607 to 775 kg/m$^2$/y or ±~10%. To reduce glaciological noise and develop a more robust, regionally representative record for the lower latitude, lower elevation (<2900 m) and moderate snow accumulation (>60 kg/m$^2$/y) DML region, annual rBC fluxes measured at the nearby B40 and NUS08_7 sites were averaged (Extended Data Fig. 1). The records from the B53 and NUS07_7 sites were combined similarly to create a representative record for the higher latitude, higher elevation (>3700 m), and low snow accumulation (<30 kg/m$^2$/y) iEAP.

**Dating the onset of enhanced rBC deposition in the nAP:** The break function regression algorithm BREAKFIT [26] was used to determine objectively the onset of rBC deposition increases in the nAP relative to continental Antarctica. Intersecting linear trends were fit to the average differences between the nAP and scaled continental deposition records from 1 to 1600 (Fig. 1). Results show (1) the onset of enhanced deposition in the nAP occurred in 1297 (±30) and (2) relative deposition increased only slightly from 1 to 1297, suggesting little change in SH BB emissions in general and particularly poleward of 40$^o$S.

**FLEXPART atmospheric aerosol and deposition modeling:** State-of-the-art FLEXPART (version 10.1) atmospheric aerosol transport and deposition [5,19] simulations were used to interpret the ice-core records. Detailed meteorological data are required for FLEXPART modeling so we used 1920 to 2000 coupled climate reanalysis for the 20$^{th}$ C (CERA-20C) conducted at the European Centre for Medium Range Weather Forecasts [44] and assumed – following similar previous studies of past aerosols changes measured in polar ice [35] – that long-range atmospheric transport was similar in the past. We employed both forward and backward FLEXPART simulations. For equivalent source-receptor geometries, backward and forward simulations are equally accurate. For short time averages, random differences can occur due to interpolation and numerical errors [19] but these are negligible for multi-decadal simulations.

Note that for quantitative analysis of ice core data, backward simulations are preferable for two reasons: 1) they are computationally more efficient; 2) they can be started directly at the ice core's point location, whereas forward simulations produce gridded receptor output.

Forward simulations were used to determine spatial patterns of rBC fallout from postulated New Zealand emissions (Fig. 3). Simulated rBC aerosols were released between the surface and 3 km in three boxes covering New Zealand (167 to 170$^{o}$E, 44 to 47$^{o}$S; 171 to 174$^{o}$E, 41 to 44$^{o}$S; 174 to 177$^{o}$E, 37 to 41$^{o}$S), with the seasonal timing of the releases each year approximating modern open BB emissions. Releases occurred between August and January corresponding to the austral spring and summer seasons, with twice the rate of rBC emissions during September.

Backward simulations were performed for the JRI, B40, B53, and NUS07_7 sites to derive emission sensitivities at 2$^{o}$ by 2$^{o}$ resolution. B40 was used to represent the DML region, while the B53 and NUS07_7 emission sensitivities were averaged to create an iEAP composite (Extended data Fig. 2). Simulated deposition at the core sites was computed by multiplying the emission sensitivity for each model grid cell (Fig. 2, Extended data Fig. 2) from backward FLEXPART simulations [19] by the corresponding emission from that cell, followed by integration over all cells in potential source regions (assumed here to be terrestrial areas in the SH other than Antarctica).

We confirmed this approach by comparing measured and simulated 1998 to 2007 average rBC deposition at six widely separated Antarctic core sites (Extended data Fig. 8), while recognizing that the spatial pattern of modern biomass burning may be somewhat different than during much of the Common Era. We selected this recent time range because, unlike historical and prehistorical periods, rBC emissions from open BB (e.g., Global Fire Emissions Database (GFED3) [45]) and anthropogenic activities (Community Emissions Data System (CEDS) [46]) are relatively well constrained (±50 to ±100%) by satellite and instrumental measurements and modern record keeping of fossil fuel consumption and other industrial activities. Results suggest that FLEXPART emission sensitivities for the Antarctic ice-core sites may be slightly high, with simulated rBC deposition about ~2.6 times higher than observed (Extended Data Fig. 8), although the large uncertainties in the modern gridded emissions preclude assignment of the observed and simulated deposition differences to incorrect emissions or emission sensitivities. Attribution of enhanced rBC emissions after the late 13$^{th}$ C to potential source regions poleward of 40$^{o}$S was based on the deposition ratio between the nAP and continental Antarctic cores (Figs. 1, 2), and comparisons between modern simulated and observed deposition ratios show good agreement (Extended Data Fig. 8). To estimate 16$^{th}$ C rBC emissions from anthropogenic burning, we assumed an overall uncertainty of ±60% in the emission sensitivities to be consistent with the ~2.6 difference in modern simulated and observed deposition.

**Constraining climate-modulated rBC emissions:** Relatively large chronology uncertainties and low sampling resolutions in Tasmanian and Patagonian lake-sediment records

preclude meaningful correlation-based comparisons with the ice records. However, variability in the ice-core deposition ratios prior to the 14th C when emissions from New Zealand were negligible and most rBC deposited at the Antarctic ice-core sites attributed using deposition ratios to SH emissions equatorward of 40$^{o}$S, provide a means to estimate limits on maximum rBC emissions from climate-modulated BB in Tasmania and Patagonia. The nAP/DML emission sensitivity ratio for Tasmania is similar to the New Zealand ratio (Fig. 2). The variability (2σ) in the nAP/scaled DML deposition ratio (Fig. 1) in the ice prior to 1300 was 0.5 or about 15% of the 38 Gg/y attributed to Māori BB during the 16$^{th}$ C, meaning any emissions from Tasmania greater than 5.7 Gg/y would have resulted in rBC fallout exceeding the 2σ background variability in the nAP/scaled DML ratio. For southernmost Patagonia poleward of 50$^{o}$S, the nAP/DML emission sensitivity ratio is more than double the ratio for Tasmania (Fig. 2), so fallout from any emissions greater than 2.8 Gg/y would have exceeded the 2σ background variability prior to 1300.

**Additional References**


29 Mulvaney, R. *et al.* Recent Antarctic Peninsula warming relative to Holocene climate and ice-shelf history. *Nature* **489**, 141-144, doi:10.1038/nature11391 (2012).

30 Abram, N. J. *et al.* Acceleration of snow melt in an Antarctic Peninsula ice core during the twentieth century. *Nature Geoscience* **6**, 404-411, doi:10.1038/ngeo1787 (2013).

31 McConnell, J. R., Aristarain, A. J., Banta, J. R., Edwards, P. R. & Simoes, J. C. 20th-Century doubling in dust archived in an Antarctic Peninsula ice core parallels climate change and desertification in South America. *Proceedings of the National Academy of Sciences of the United States of America* **104**, 5743-5748, doi:10.1073/pnas.0607657104 (2007).

32 McConnell, J. R. *et al.* Antarctic-wide array of high-resolution ice core records reveals pervasive lead pollution began in 1889 and persists today. *Scientific Reports* **4**, doi:10.1038/srep05848 (2014).

33 Sigl, M. *et al.* Insights from Antarctica on volcanic forcing during the Common Era. *Nature Climate Change*, 693-697, doi:10.1038/NCLIMATE2293 (2014).

34 McConnell, J. R. Continuous ice-core chemical analyses using inductively Coupled Plasma Mass Spectrometry. *Environmental Science & Technolology* **36**, 7-11, doi:10.1021/es011088z (2002).

35 McConnell, J. *et al.* Lead pollution recorded in Greenland ice indicates European emissions tracked plagues, wars, and imperial expansion during antiquity. *Proceedings of the National Academy of Sciences of the United States of America* **115**, 5726-5731, doi:10.1073/pnas.1721818115 (2018).

36 Sigl, M. *et al.* Timing and climate forcing of volcanic eruptions for the past 2,500 years. *Nature* **523**, 543–549, doi:10.1038/nature14565 (2015).

37 O'Hare, P. *et al.* Multiradionuclide evidence for an extreme solar proton event around 2,610 BP (similar to 660 BC). *Proceedings of the National Academy of Sciences of the United States of America* **116**, 5961-5966, doi:10.1073/pnas.1815725116 (2019).

38 Arienzo, M. *et al.* A Method for Continuous $^{239}$Pu Determinations in Arctic and Antarctic Ice Cores. *Environ Sci Technol* **50**, 7066-7073, doi:10.1021/acs.est.6b01108 (2016).

39 McConnell, J. R. *et al.* Extreme climate after massive eruption of Alaska's Okmok volcano in 43 BC and its effects on the civil wars of the late Roman Republic. *Proceedings of the National Academy of Sciences of the United States of America*, doi:10.1073/pnas.2002722117 (2020).

40 Narcisi, B., Petit, J. R., Delmonte, B., Basile-Doelsch, I. & Maggi, V. Characteristics and sources of tephra layers in the EPICA-Dome C ice record (East Antarctica): Implications for past atmospheric circulation and ice core stratigraphic correlations. *Earth and Planetary Science Letters* **239**, 253-265, doi:10.1016/j.epsl.2005.09.005 (2005).

41 Basile, I., Petit, J. R., Touron, S., Grousset, F. E. & Barkov, N. Volcanic layers in Antarctic (Vostok) ice cores: Source identification and atmospheric implications. *Journal of Geophysical Research: Atmospheres* **106**, 31915-31931, doi:10.1029/2000JD000102 (2001).

42 Castellano, E. *et al.* Volcanic eruption frequency over the last 45 ky as recorded in Epica-Dome C ice core (East Antarctica) and its relationship with climatic changes. *Global and Planetary Change* **42**, 195-205, doi:10.1016/j.gloplacha.2003.11.007 (2004).

43 Cole-Dai, J. *et al.* Comprehensive Record of Volcanic Eruptions in the Holocene (11,000 years) From the WAIS Divide, Antarctica Ice Core. *Journal of Geophysical Research: Atmospheres* **126**, e2020JD032855, doi:10.1029/2020JD032855 (2021).

44 Laloyaux, P., de Boisseson, E. & Dahlgren, P. CERA-20C: An Earth system approach to climate reanalysis. *ECMWF Newsletter* **150**, 25-30 (2017).

45 van der Werf, G. R. *et al.* Global fire emissions and the contribution of deforestation, savanna, forest, agricultural, and peat fires (1997–2009). *Atmos. Chem. Phys.* **10**, 11707-11735, doi:10.5194/acp-10-11707-2010 (2010).

46 Hoesly, R. M. *et al.* Historical (1750–2014) anthropogenic emissions of reactive gases and aerosols from the Community Emissions Data System (CEDS). *Geosci. Model Dev.* **11**, 369-408, doi:10.5194/gmd-11-369-2018 (2018).

47 Bisiaux, M. M. *et al.* Variability of black carbon deposition to the East Antarctic Plateau, 1800–2000 AD. *Atmos. Chem. Phys.* **12**, 3799-3808, doi:10.5194/acp-12-3799-2012 (2012).

48 Bisiaux, M. M. *et al.* Changes in black carbon deposition to Antarctica from two high-resolution ice core records, 1850–2000 AD. *Atmos. Chem. Phys.* **12**, 4107-4115, doi:10.5194/acp-12-4107-2012 (2012).

49 Le Bas, M. J., Le Maitre, R. W., Streckeisen, A., Zanettin, B. & Rocks, I. S. o. t. S. o. I. A Chemical Classification of Volcanic Rocks Based on the Total Alkali-Silica Diagram. *Journal of Petrology* **27**, 745-750, doi:10.1093/petrology/27.3.745 (1986).

50 Palais, J. M., Kyle, P. R., Mosley-Thompson, E. & Thomas, E. Correlation of a 3,200 year old tephra in ice cores from Vostok and South Pole Stations, Antarctica. *Geophysical Research Letters* **14**, 804-807, doi:10.1029/GL014i008p00804 (1987).

51 Kyle, P. R., Palais, J. & Thomas, E. The Vostok tephra - An important englacial stratigraphic marker? *Antarctic Journal U.S.* **19**, 64-65 (1984).

**Acknowledgements:** National Science Foundation (NSF) grants 0538416, 0968391, 1702830, 1832486, and 1925417 to J.R.M. funded this research, with internal funding provided by DRI for laboratory analyses of the two JRI cores. Additional funding from NSF 1702814 supported P.L. and Swiss National Science Foundation grant P400P2_199285 supported S.O.B. We thank all the British, French, Argentine, German, Norwegian, Australian, and American field teams for their efforts, as well as students and staff in the DRI ice-core group, for assistance in the laboratory.

**Author Contributions** J.R.M. designed the study, with contributions from N.J.C., A.S., G.P., D.B.M., and P.L. J.R.M., R.M, S.K., E.I., A.J.A., N.J.A, and D.B.M. provided ice samples and previous measurements. J.R.M., N.J.C., R.M., G.P., S.K., J.F., K.E.G., and S.O.B. conducted and analyzed measurements. R.M., S.E., and P.L. conducted model simulations. J.R.M., N.J.C., A.S., G.P., and D.B.M led the writing of the manuscript and all other co-authors contributed.

**Competing Interests** The authors declare no competing interests.

**Additional Information** Supplementary Information is available for this paper.

**Correspondence and requests for materials** should be addressed to J.R.M.

**Extended data** is available for this paper.

## Extended Data Figure Legends

**Extended Data Figure 1 | rBC fluxes and concentrations measured in the Antarctic ice-core array. a,b,** JRI records used to represent the nAP. rBC measurements of the JRI_D98 record (red) from 2007 confirm 2016 measurements in the JRI_2008 core (black) (Methods). **c-g,** The B40 and scaled NUS08_7 records were averaged to create a DML regional composite. **h-l,** The B53 and scaled NUS07_7 cores were combined to create an iEAP regional composite. Shown are annual (light) and 11-year geometric mean filtered (heavy) fluxes.

**Extended Data Figure 2 | FLEXPART-simulated emission sensitivities. a,** nAP. **b,** iEAP. **c,** nAP/iEAP. **d,** nAP-iEAP, where the iEAP scaler of 10.1 is the average nAP/iEAP ratio in the ice cores from 900 to 1200. Insets show values for New Zealand and crosses mark ice-core locations.

**Extended Data Figure 3 | Comparison of original 2013 and selected replicate 2016 rBC measurements in the B40 ice core.** Parallel B40 samples either from **a,** shallower firn and **b,** deeper ice were measured at the start of each day to monitor any changes in calibrations or instrument responses during the 2016 analysis of the JRI_2008 core.

**Extended Data Figure 4 | Example of annual layer counting using new high-resolution elemental and chemical measurements over the full 363.9-m depth of the JRI_2008 core.** Corresponding years are shown along the top. Previous high-resolution measurements extended only to 130 m so annual layer counted ended at ~1807 [30]. Here we extended annual layer counting to ~300 m or ~1000.

**Extended Data Figure 5 | Evaluation of ice-core chronology consistency during the 12$^{th}$ C through 18$^{th}$ C using sulfur fallout from explosive volcanism.** Shown are annually averaged sulfur concentrations in the five longer ice cores in the Antarctic rBC array. The average of the four continental cores (**b**-**e**) is shown in light gray for perspective. Also shown are tie points for this time range used to constrain annual layer counting and ice flow modeling in the JRI_2008 record.

**Extended Data Figure 6 | Revised depth-age scale and modeled water flux for the JRI_2008 ice core on the WD2014 age scale. a,** The chronology (black solid) is based on annual layer counting (red dashed) from the surface to ~275 m (corresponding to 2008 to 1257) and ice flow modeling from ~275 m to the bottom, although annual layer counting is possible to ~300 m corresponding to the year 1000. Flow modeling is constrained by 12 depth-age control points (diamonds) including the Vostok tephra at 345.43 m also found in East Antarctic cores and dated to 3568 YPB. The control points below 350 m depth are 358.627 m, 11988 YBP; 358.785 m, 12800 YBP; and 359.000 m, 14607 YBP). **b,** Water flux.

**Extended Data Figure 7 | Total alkali silica plot [49] illustrating similarity of the tephra shards extracted from 345.43 m in the JRI_2008 core to the Vostok tephra and its correlatives previously reported in a number of cores from Vostok [40,50,51], South Pole [51], and Dome**

**Concordia [41].** Geochemical fields are based on Narcisi et al. [40] We determined an eruption date of 3568 yBP on the WD2014 age scale by synchronizing high-resolution sulfate measurements to continuous sulfate measurements in WAIS Divide.

**Extended Data Figure 8 | Observed and predicted rBC deposition and deposition ratio relative to B40 from 1998 to 2007 at widely spaced Antarctic ice core sites. a** Drilling locations (Extended Data Table 1). Observed and predicted **b** deposition and **c** deposition ratio (Figs. 1,2).

## Extended Data Table Title

**Extended Data Table 1| Location and other details for Antarctic ice cores.**

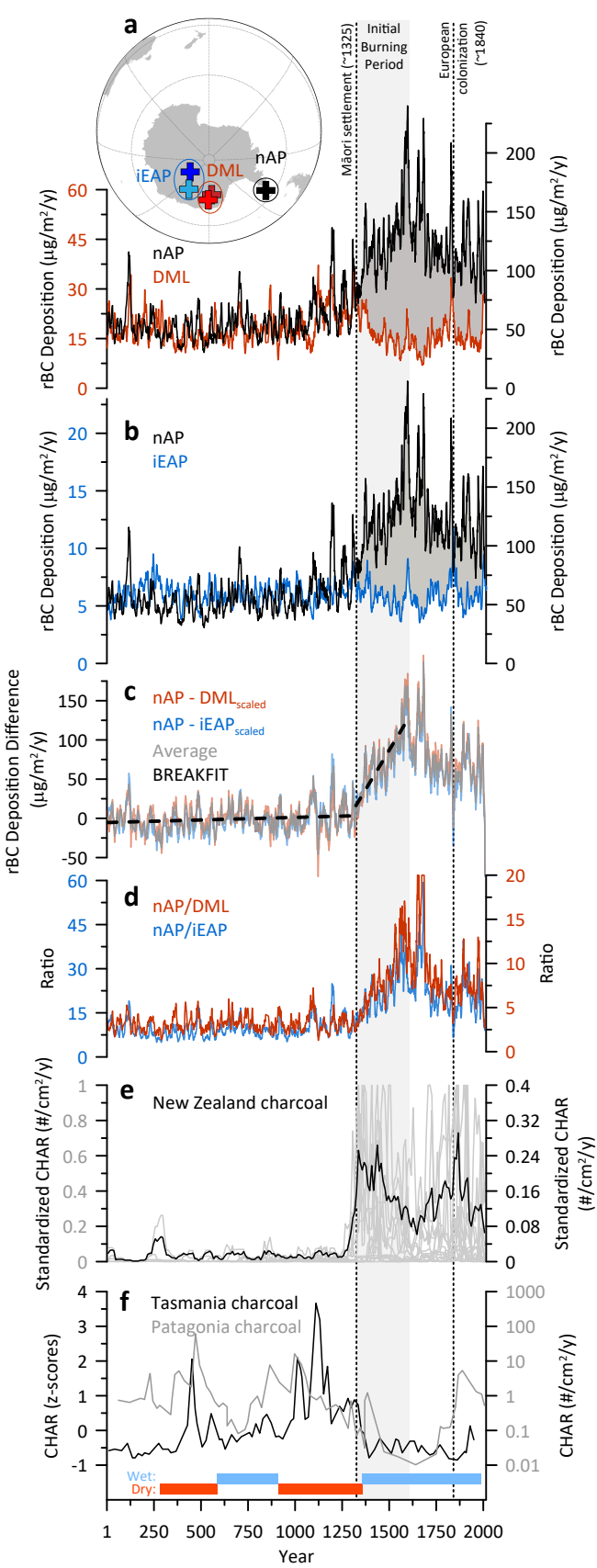
a
iEAP
DML
nAP
Māori settlement (~1325)
Initial Burning Period
European colonization (~1840)
rBC Deposition (µg/m²/y)
nAP
DML
b
nAP
iEAP
c
nAP - DML scaled
nAP - iEAP scaled
Average
BREAKFIT
rBC Deposition Difference (µg/m²/y)
d
nAP/DML
nAP/iEAP
Ratio
e
New Zealand charcoal
Standardized CHAR (#/cm²/y)
f
Tasmania charcoal
Patagonia charcoal
CHAR (z-scores)
CHAR (#/cm²/y)
Wet:
Dry:
1
250
500
750
1000
1250
1500
1750
2000
Year

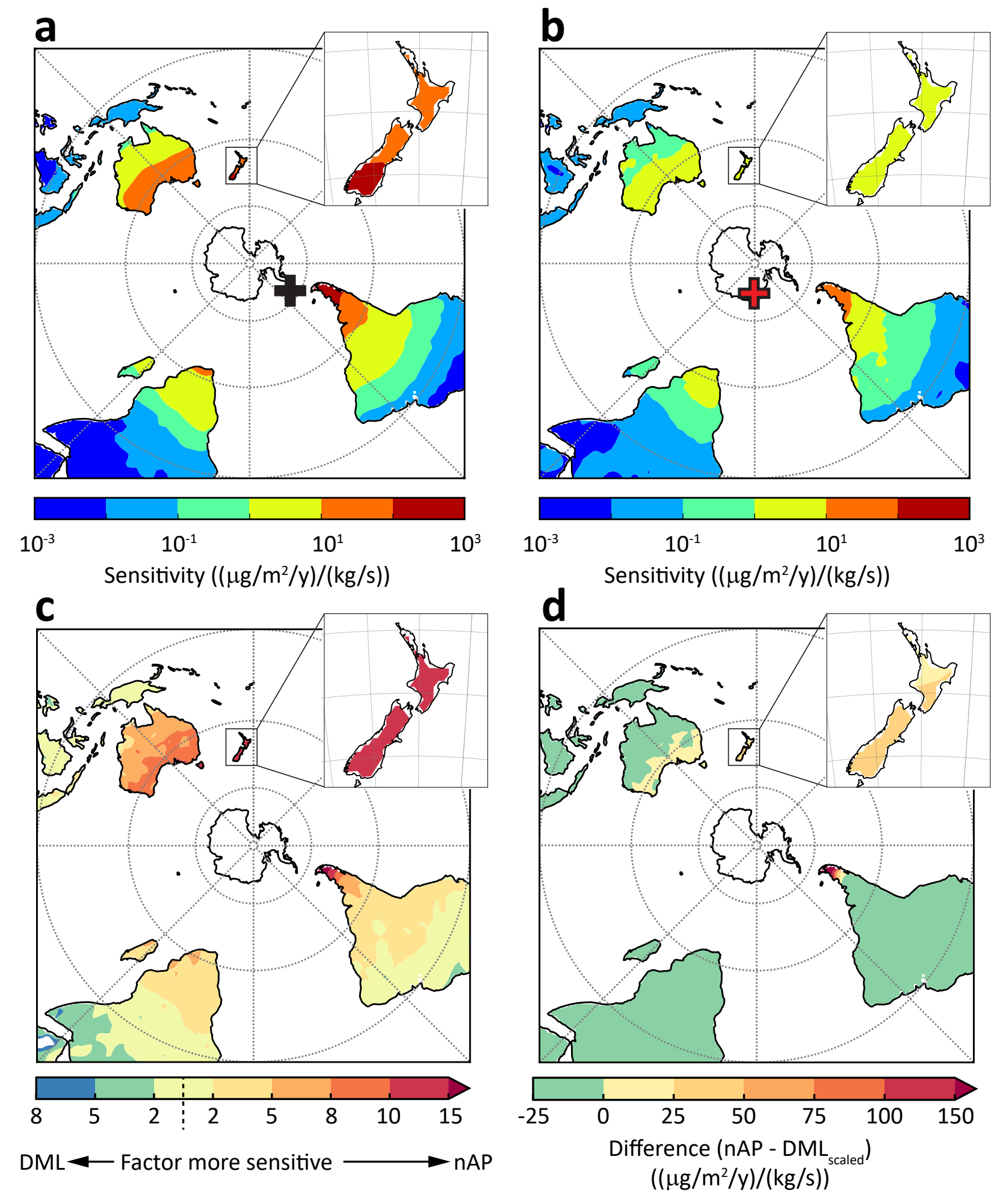
a
b
c
d
10-3
10-1
101
103
Sensitivity ((µg/m2/y)/(kg/s))
8
5
2
2
5
8
10
15
DML
Factor more sensitive
nAP
-25
0
25
50
75
100
150
Difference (nAP - DMLscaled)
((µg/m2/y)/(kg/s))

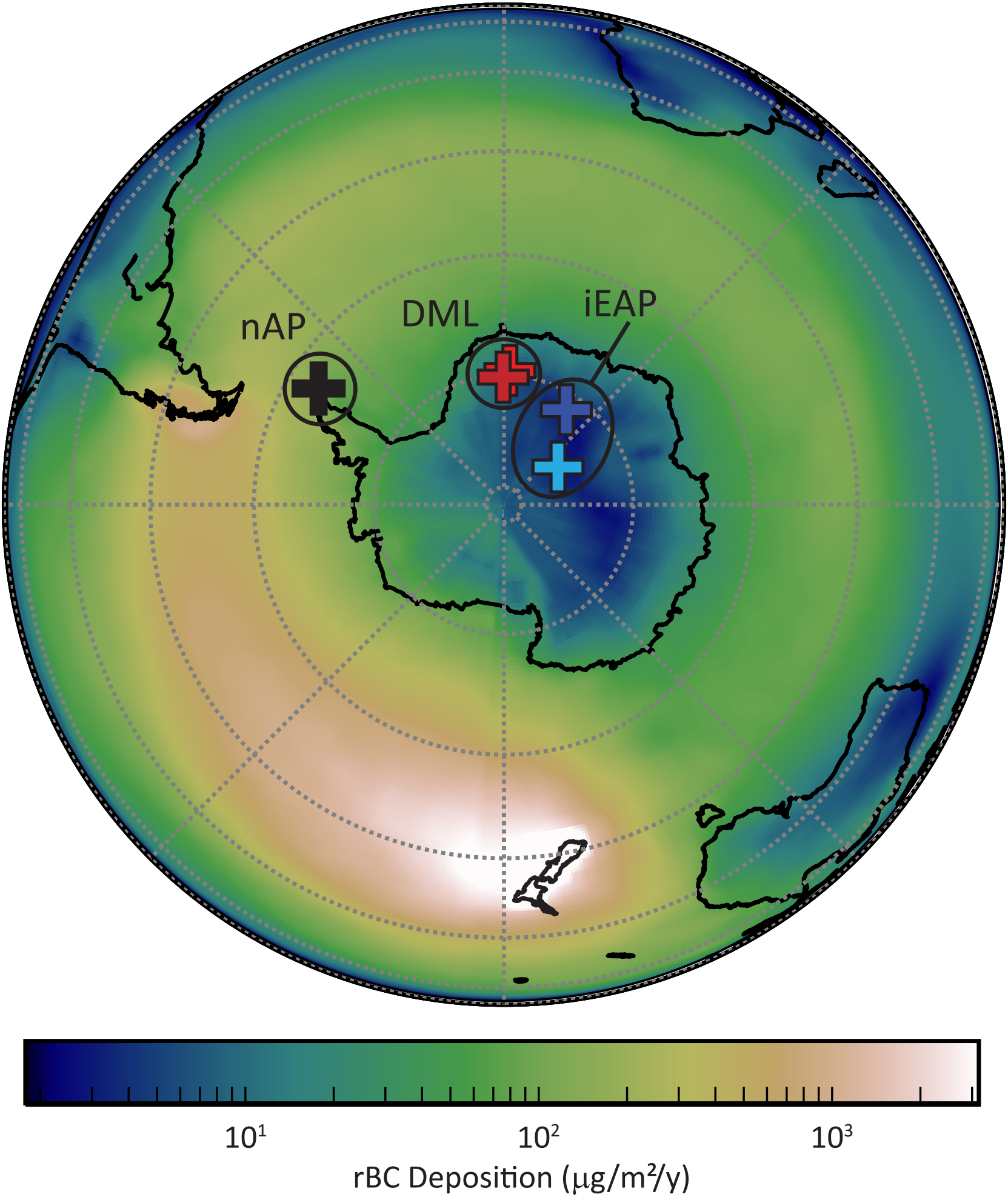
nAP
DML
iEAP
$10^1$
$10^2$
$10^3$
rBC Deposition (μg/m²/y)

| Ice Core Site | Latitude (deg N) | Longitude (deg E) | Elevation (m) | Recent snowfall (kg/m²/y) | Year analyzed | References | |
|---|---|---|---|---|---|---|---|
| | | | | | | rBC measurements | Chronology |
| James Ross Island JRI_2008 | -64.2 | -57.7 | 1542 | 630 | 2016 | 1750 to PD [9]<br>1 to 1750 (This study) | (This study) |
| James Ross Island JRI_D98 | -64.2 | -57.7 | 1580 | 630 | 2007 | (This study) | (This study) |
| B40 | -75 | 0.1 | 2891 | 68 | 2013 | 1 to PD [16] | [33, 36] |
| NUS08_7 | -74.1 | 1.6 | 2700 | 86 | 2010 | 1750 to PD [9]<br>1 to 1750 (This study) | [33] |
| B53 | -76.8 | 31.9 | 3729 | 29 | 2017 | 1750 to PD [9]<br>1 to 1750 (This study) | (This study) |
| NUS07_7 | -82.1 | 54.9 | 3725 | 30 | 2018 | 1800 to PD [47]<br>1750 to PD [9]<br>1 to 1750 (This study) | [33] |
| WAIS Divide | -79.5 | -112.1 | 1759 | 210 | 2008/9 | 1850 to PD [48]<br>1750 to PD [9] | [36] |
| ABN | -77.2 | 111.4 | 2700 | 119 | 2014/2015 | [9] | [9] |

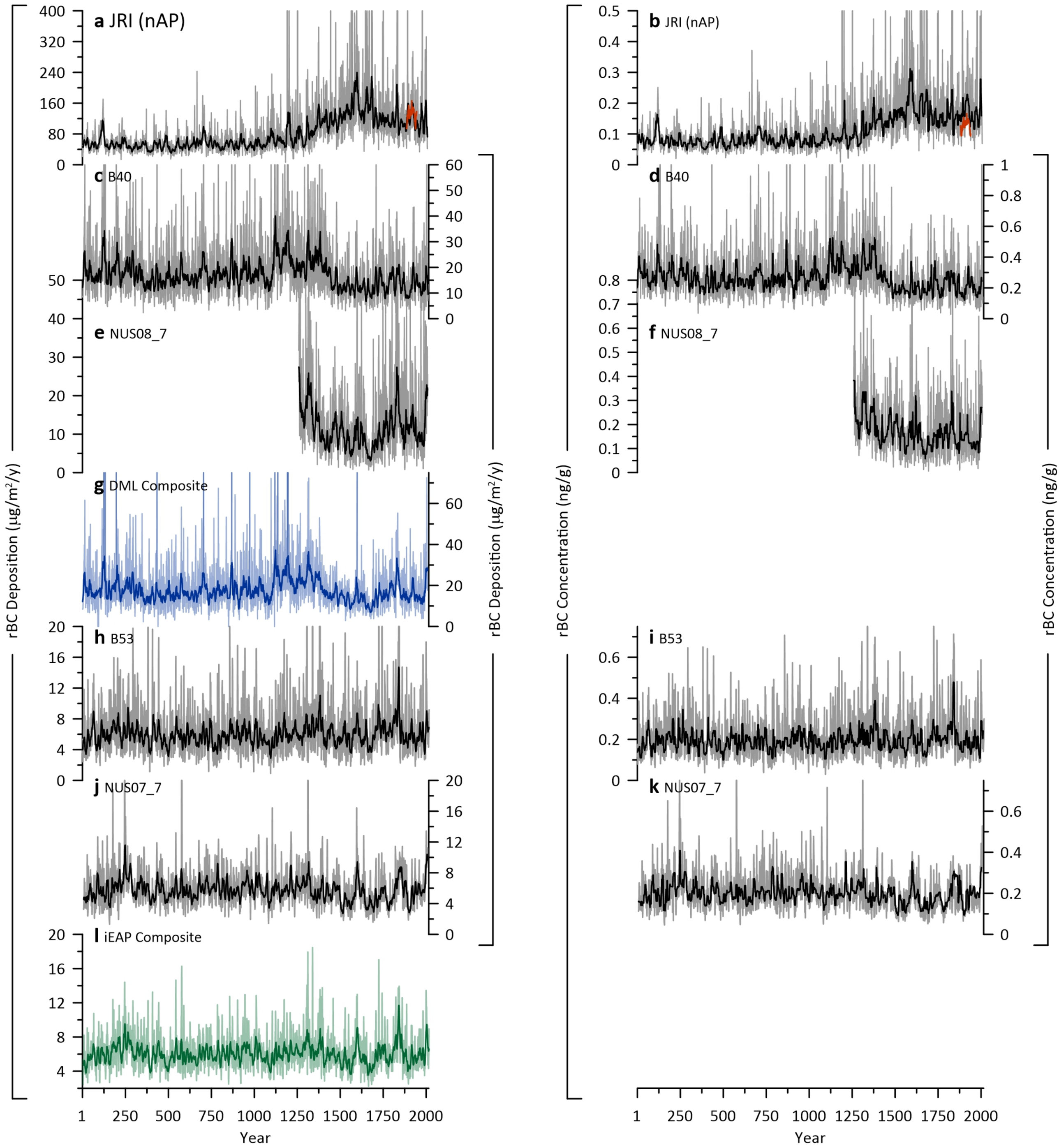
a JRI (nAP)
b JRI (nAP)
c B40
d B40
e NUS08_7
f NUS08_7
g DML Composite
h B53
i B53
j NUS07_7
k NUS07_7
l iEAP Composite
rBC Deposition (µg/m²/y)
rBC Concentration (ng/g)
Year

a

b

$10^{-3}$ $10^{-1}$ $10^{1}$ $10^{3}$

Sensitivity ((μg/m²/y)/(kg/s))

c

d

2 2 5 15 30 50

iEAP ← Factor more sensitive → nAP

-25 0 25 50 75 100 150

Difference (nAP - $iEAP_{scaled}$)
((μg/m²/y)/(kg/s))

a

Original
1/13/2016
1/20/2016
1/21/2016

rBC concentration (ng/g)

0
0.1
0.2
0.3
0.4
0.5
0.6
0.7
0.8
0.9
1

30
31
32
33
34
35
36

Depth (m)

b

Original
2/3/2016
2/2/2016
2/1/2016
1/28/2016

rBC concentration (ng/g)

0
0.2
0.4
0.6
0.8
1
1.2
1.4
1.6
1.8
2

82
83
84
85
86
87

Depth (m)

1332 1331 1330 1329 1328 1327 1326 1325 1324 1323 1322 1321 1320 1319 1318 1317

-0.4 -0.8 -1.2 -1.6 -2 -2.4 -2.8 -3.2

$\ln(NH_4^+$ [um])

1.5 1 0.5 0 -0.5 -1 -1.5 -2 -2.5 -3 -3.5

ln(nssS/ssNa)

224 224.2 224.4 224.6 224.8 225 225.2 225.4 225.6 225.8 226

Depth (m weq)

JRI tie points:

**a** JRI

Sulfur (ng/g)

**b** B53

Sulfur (ng/g)

**c** NUS07_7

Sulfur (ng/g)

**d** B40

Sulfur (ng/g)

**e** NUS08_7

Sulfur (ng/g)

Year

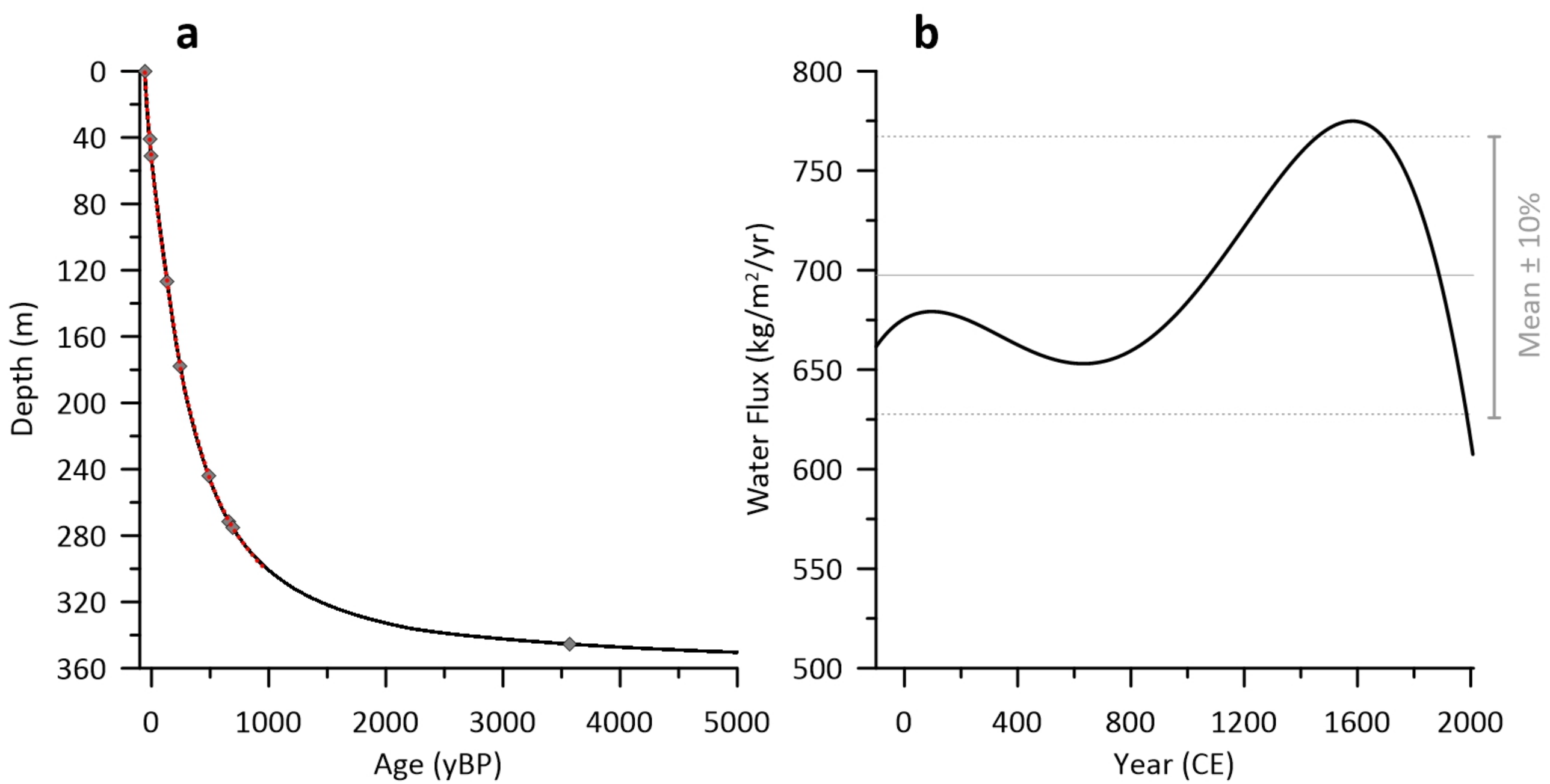
a
0
40
80
120
160
200
240
280
320
360
Depth (m)
0
1000
2000
3000
4000
5000
Age (yBP)
b
800
750
700
650
600
550
500
Water Flux (kg/m²/yr)
0
400
800
1200
1600
2000
Year (CE)
Mean ± 10%

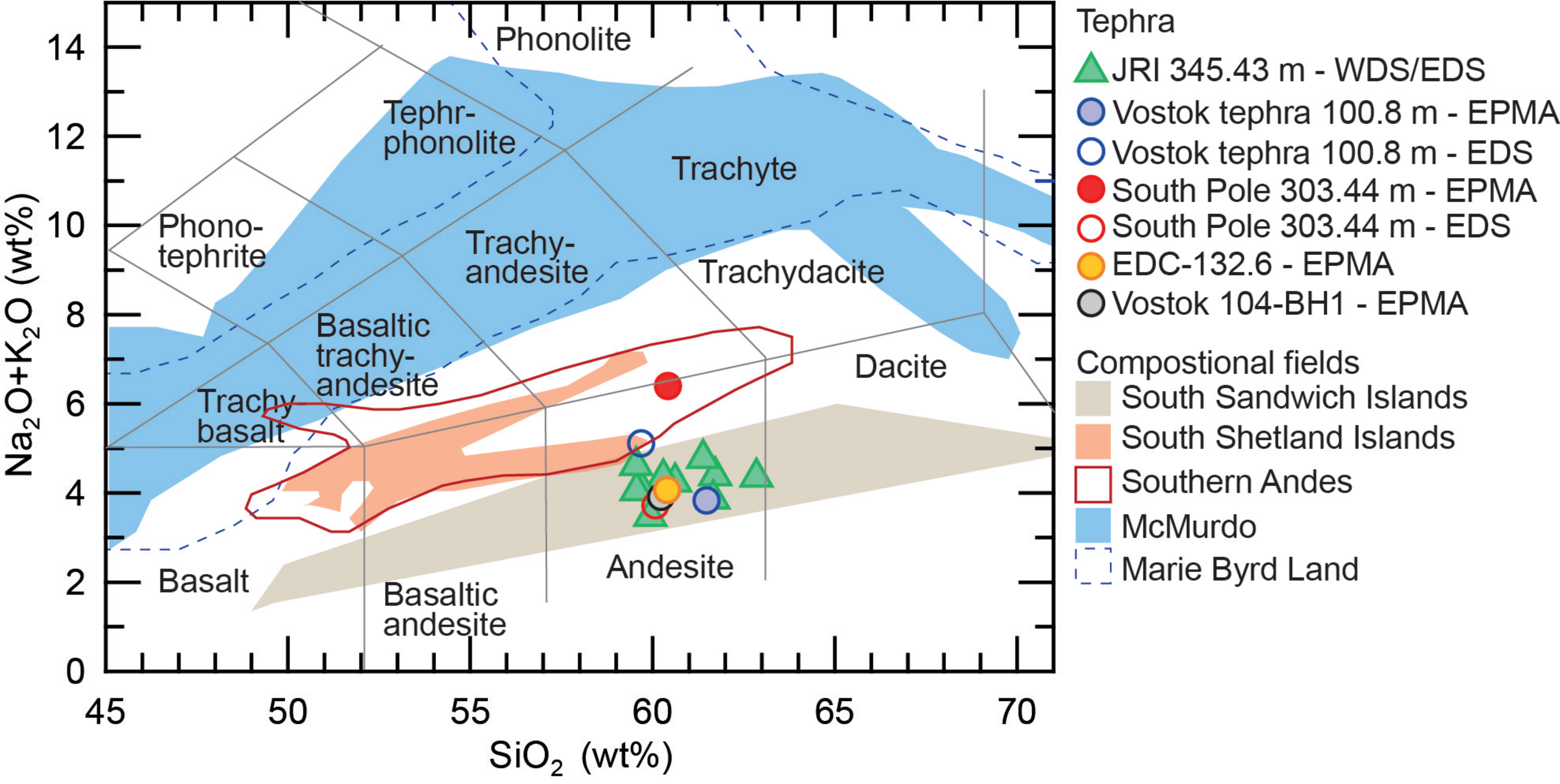
Phonolite
Tephr-
phonolite
Trachyte
Phono-
tephrite
Trachy-
andesite
Trachydacite
Basaltic
trachy-
andesite
Dacite
Trachy
basalt
Andesite
Basalt
Basaltic
andesite
14
12
10
8
6
4
2
0
45
50
55
60
65
70
$Na_2O+K_2O$ (wt%)
$SiO_2$ (wt%)
Tephra
JRI 345.43 m - WDS/EDS
Vostok tephra 100.8 m - EPMA
Vostok tephra 100.8 m - EDS
South Pole 303.44 m - EPMA
South Pole 303.44 m - EDS
EDC-132.6 - EPMA
Vostok 104-BH1 - EPMA
Compostional fields
South Sandwich Islands
South Shetland Islands
Southern Andes
McMurdo
Marie Byrd Land

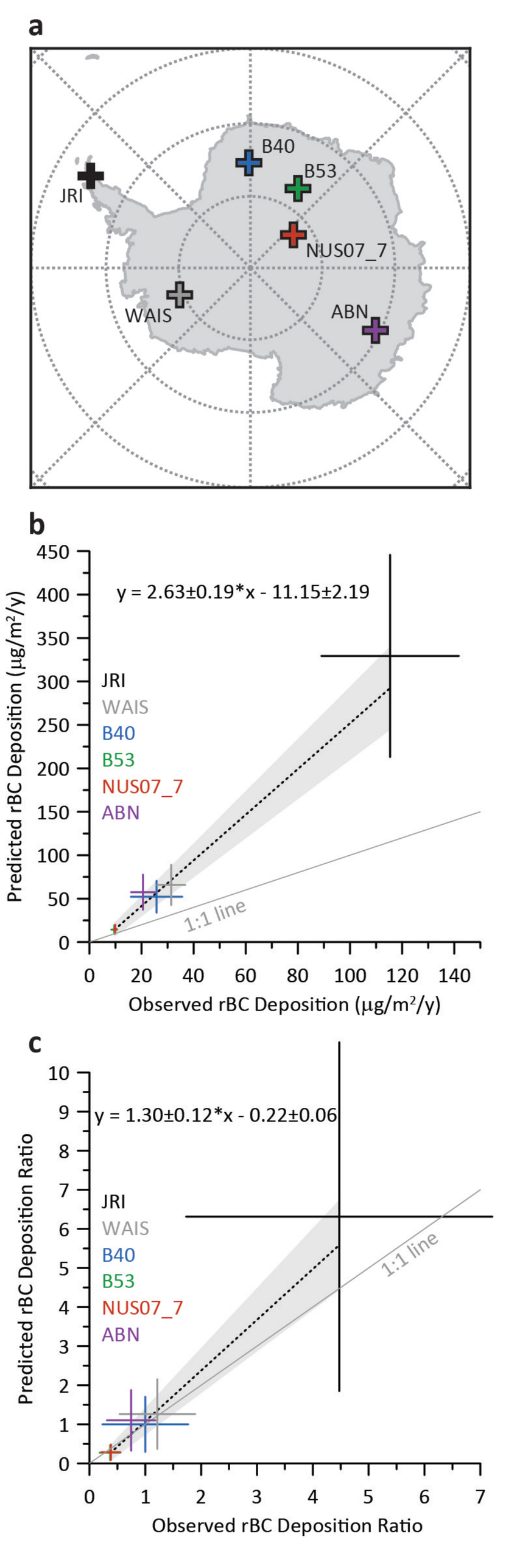
a
B40
B53
JRI
NUS07_7
WAIS
ABN
b
y = 2.63±0.19*x - 11.15±2.19
JRI
WAIS
B40
B53
NUS07_7
ABN
1:1 line
Predicted rBC Deposition (µg/m²/y)
Observed rBC Deposition (µg/m²/y)
0
50
100
150
200
250
300
350
400
450
0
20
40
60
80
100
120
140
c
y = 1.30±0.12*x - 0.22±0.06
JRI
WAIS
B40
B53
NUS07_7
ABN
1:1 line
Predicted rBC Deposition Ratio
Observed rBC Deposition Ratio
0
1
2
3
4
5
6
7
8
9
10
0
1
2
3
4
5
6
7